Laterally Resolved Orientation and Film Thickness of Polar Metal Chlorine Phthalocyanines on Au and ITO

ARTICLE *in* THE JOURNAL OF PHYSICAL CHEMISTRY C · MAY 2011

Impact Factor: 4.77 · DOI: 10.1021/jp202412y

8 AUTHORS, INCLUDING:

Heiko Peisert
University of Tuebingen
127 PUBLICATIONS **2,622** CITATIONS
SEE PROFILE

Umut Aygül
University of Tuebingen
14 PUBLICATIONS **168** CITATIONS
SEE PROFILE

Fotini Petraki
28 PUBLICATIONS **403** CITATIONS
SEE PROFILE

Tamara Basova
Nikolaev Institute of Inorganic Chemistry, SB…
123 PUBLICATIONS **976** CITATIONS
SEE PROFILE

THE JOURNAL OF PHYSICAL CHEMISTRY C

ARTICLE

pubs.acs.org/JPCC

Laterally Resolved Orientation and Film Thickness of Polar Metal Chlorine Phthalocyanines on Au and ITO

Florian Latteyer,*[,†] Heiko Peisert,[†] Umut Aygül,[†] Indro Biswas,[†] Fotini Petraki,[†] Tamara Basova,[§] Antje Vollmer,[‡] and Thomas Chassé[†]

[†]Institute for Physical and Theoretical Chemistry, Auf der Morgenstelle 18, 72076 Tübingen, Germany

[‡]Helmholtz Zentrum Berlin für Materialien und Energie, Elektronenspeicherring BESSY II, Albert-Einstein-Strasse 15, 12489 Berlin, Germany

[§]Nikolaev Institute of Inorganic Chemistry, Novosibirsk, Russia

ABSTRACT: The molecular orientation and homogeneity of gallium(III) and aluminum(III) chlorine phthalocyanine (GaClPc and AlClPc) are studied on flat (gold single crystal, Au(100)) and rough surfaces (indium tin oxide, ITO) by Raman spectroscopy in combination with X-ray absorption spectroscopy (XAS) in detail. In the case of Raman spectroscopy, Euler angles are used to describe the geometry while Raman imaging provides insight into homogeneity. For XAS, synchrotron radiation is applied to study the angle dependence of the excitation structure. On Au(100) the molecules are highly ordered and tend to align parallel to the surface (lying) with a layer by layer growth mode. Contrarily, on technically relevant substrates, as in the case of ITO, less ordered films due to the roughness of the surface nature are present. The results are discussed in relation to the substrate's nature and the influence of dipole moments.

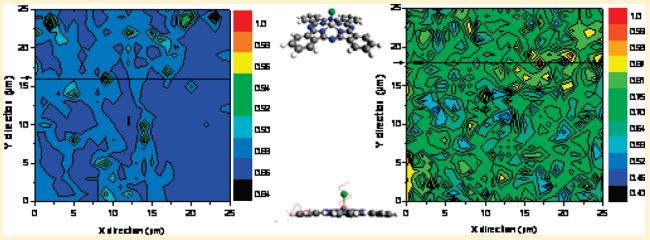

1. INTRODUCTION

Phthalocyanines (Pcs) are one of the most studied organic semiconductors. They are well suited for several applications,[1−10] utilizing often their semiconducting properties as active layers for organic light emitting diodes (OLEDs),[1] solar cells,[1−3] sensors,[4−6] or field effect transistors (OFETs).[7,8] High chemical stability and easy functionalization at the benzene ring (e.g., due to peripheral substitution by a variety of side chains) and at the central metal are key properties. Furthermore, their physical and chemical properties can be tailored over a wide range. For example, the change of the central metal atom in the Pc molecule significantly varies the electronic properties of the bulk material and of the corresponding interfaces.[11,12]

The importance of controlling properties for many of the above-mentioned applications, such as growth,[13,14] molecular orientation,[15−20] interface properties,[16,20−23] and electronic properties,[16,24−26] is demonstrated. It is necessary to control these parameters in order to optimize device efficiency and behavior. In a recent work a possible alignment of AlClPc with an external electric field is shown.[27] As an example, CuPc and ZnPc are one of the most investigated molecules of the phthalocyanine class. Growth mechanisms[13,14] on different substrates as well as in heterojunctions[1,28] are studied intensively. Different experimental methods with considerable effort are applied to understand the physical and chemical behavior for applications of phthalocyanines such as vibrational techniques,[5,15,18] X-ray methods,[16,17] and conductivity measurements.[29]

Although CuPc is a flat molecule exhibiting D_{4h} symmetry, the central metal in GaClPc is not in plane with the phthalocyanine ring. This leads to a deformation of approximately 7° and symmetry lowering to C_{4v} (structural equivalent to VOPc, TiOPc, and AlClPc). For instance, investigations on Ga substituted phthalocyanines such as theoretical methods,[30] triplet−triplet annihilation by photophysics,[31] and other photochemical properties[32,33] such as tumor uptake[34] and annealing effects[35] have already been presented.

Here, a study of the orientation of GaClPc and AlClPc at the interface of Au(100) and ITO is presented. As noted above, the orientation properly affects the electronic and interface properties. For instance, a parallel orientation related to the surface in organic solar cells increases the mobility of charges, while in contrast in organic field effect transistors a perpendicular orientation leads to a higher mobility in the conduction channels. In this context, XAS and polarized Raman spectroscopy are quite convenient methods in order to probe the geometry close to the substrate surface. Two types of substrates have been chosen: an atomically flat surface (as model surface) and a rough surface of technical relevance due to the fact that polar Pcs are mostly studied on single crystalline substrates.

2. EXPERIMENTAL SECTION

2.1. Materials. The organic materials GaClPc and AlClPc were purchased from Sigma Aldrich Schnelldorf, Germany. The

Received: March 14, 2011
Revised: May 4, 2011

   dx.doi.org/10.1021/jp202412y | J. Phys. Chem. C XXXX, XXX, 000–000

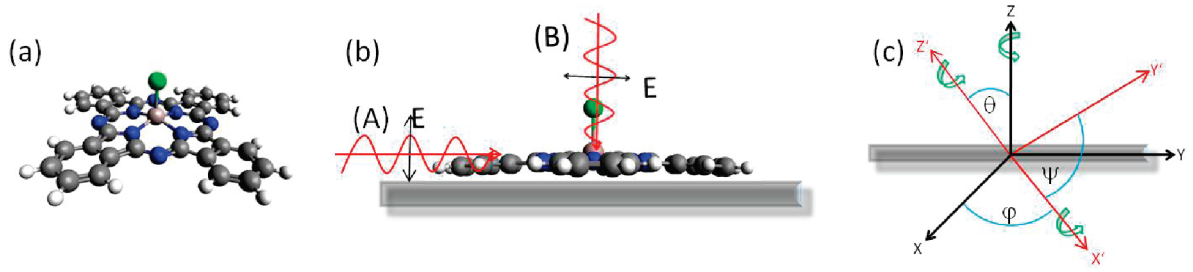

Figure 1. (a) Structure of M(III) chloride phthalocyanine (M = Ga, Al). Atom colors are explained in the text. (b) Illustration of different inclinations in p-polarization (A) grazing incidence of the electric field vector **E** with respect to the substrate normal. (B) Normal incidence of the electric field vector **E**. (c) Visualization of the Euler angles. φ is the rotation around the global Z-axis, θ the rotation around the molecular X'-axis (tilt angle between Z and Z'), and ψ the rotation around the molecular Z'-axis.

GaClPc was used without any further purification. AlClPc was purified by gradient sublimation in ultrahigh vacuum (UHV) at 1×10^{-9} mbar in order to avoid dimerization of AlClPc which is triggered by the presence of water.[36] Cleanliness and composition have been controlled using X-ray photoemission spectroscopy (XPS) and Raman spectroscopy. Figure 1(left) presents the molecular structure (as a ball-and-stick-model). Atoms appear in different colors—hydrogen, white; carbon, gray; nitrogen, blue; gallium/aluminum, rose; chlorine, green.

In comparison with planar phthalocyanines (e.g., the prominent CuPc), GaClPc and AlClPc possess comparably large dipole moments. These have been calculated (B3LYP/6-311G(d,p))[37] to be 1.2976×10^{-29} C·m (3.89 D) for both AlClPc and GaClPc molecules. These dipole moments are about two times larger than the dipole moment of water.

2.2. Methods. XAS measurements (also known as near edge X-ray absorption fine structure (NEXAFS)) are performed at the synchrotron facility BESSY II of the Helmholtz-Zentrum Berlin using the Optics-beamline and the end station SurICat (base pressure of 1×10^{-10} mbar). All spectra were recorded with p-polarized light (Figure 1b).[38] At the N 1s edge (photon energy of about 400 eV), the energy resolution was approximately 80−100 meV. The absorption spectra were measured by recording the sample current with a high precision Keithley picoamperemeter (model 2400) in total electron yield (TEY). Normalization of XAS spectra to equal edge step heights is necessary in order to compare the near edge resonance structures. The raw data have been corrected according to established procedures.[16,38]

Raman spectra are recorded using a Horiba Jobin LabRam HR800 confocal spectrometer equipped with a BX 41 microscope. The applied lens yields a magnification of 100-fold with a numerical aperture (NA) of 0.9. The spatial resolution (central lobe diameter) for this lens is approximately 0.7 μm, and the estimated field depth is calculated to be 3.2 μm (assuming $n = 1.2$ for Pcs[39]).[40] Concerning the much smaller film thicknesses (<10 nm), the complete film is probed by the confocal volume. Collecting Raman spectra in parallel and perpendicular polarization (with respect to the incident laser polarization vector) enables determination of depolarization ratios.

The spectra are recorded in backscattering geometry using a Nd:YAG laser with an excitation wavelength of 532 nm. This wavelength is beyond the absorption range for both molecules according to UV/vis spectroscopic data (not shown). Thus, one can neglect the contribution of resonance enhancement, which would complicate the determination of the molecular orientation from the depolarization ratio (e.g., due to a symmetry distortion[41]). An edge filter disrupts the Rayleigh line up to 120 cm^{-1}. To prevent radiation damage in advance the laser intensity is attenuated by 90% by using a D1 filter (1.6 mW).

Gratings with 600 lines mm^{-1} for overview and 1800 lines mm^{-1} for detailed spectra are used. The spectral resolution accounts to 2.5 cm^{-1}.

A motorized xy stage is applied for Raman mapping; the smallest step size is 100 nm. Due to the resolution described above, a 25 × 25 μm^2 area is scanned with a step size of 1 μm. Under these circumstances one Raman image contains 676 single spectra. In this process the z distance of the microscope is kept fix related to the substrate surface. The backscattered intensity strongly depends on either the quantity of molecules in the central lobe or the molecular orientation. Changes in intensities can then draw a picture of the surface nature (e.g., terraces, islands, edges), within the given resolution parameters.

The Au (100) single crystal is prepared by multiple cycles of Ar^+ ion sputtering and annealing which facilitate highly ordered surfaces. This is confirmed by low energy electron diffraction (LEED) whereby a (5 × 20) surface reconstruction is observed (not shown). For the cleaning of ITO, rinsing ex situ with acetone and ethanol and in situ with several cycles of annealing without sputtering is applied as the sputtering procedure may significantly alter the surface composition by loss of oxygen. To check the cleanliness of the substrates, X-ray photoemission spectroscopy (XPS) and LEED are applied. The XPS spectra clearly show the electronic structure, but they do not contribute to the orientation and homogeneity analysis and are thus not shown here.

Thin films are prepared in ultrahigh vacuum (base pressure $<1 \times 10^{-9}$ mbar). Monitoring of the evaporation from a temperature controlled cell with (i) a quartz microbalance monitor (Inficon XTM/2) (between 1 and 2 nm min^{-1}) and (ii) cross checks evaluating XPS intensity ratios allow film thickness estimation.

3. ANALYSIS OF MOLECULAR ORIENTATION

3.1. XAS. One advantage of synchrotron light is the high linear polarization of the electric field vector **E**. Exploiting this, incidence angle and polarized excitations from the occupied core levels to unoccupied states can be probed as a function of the energy (Figure 1b). Those excitations are subject to selection rules such as the change of the quantum number of the angular momentum ($\Delta l = \pm 1$). Thus, for organic molecules, transitions from N 1s or C 1s orbitals into both π^* and σ^* molecular orbitals are allowed.

dx.doi.org/10.1021/jp202412y |J. Phys. Chem. C XXXX, XXX, 000–000

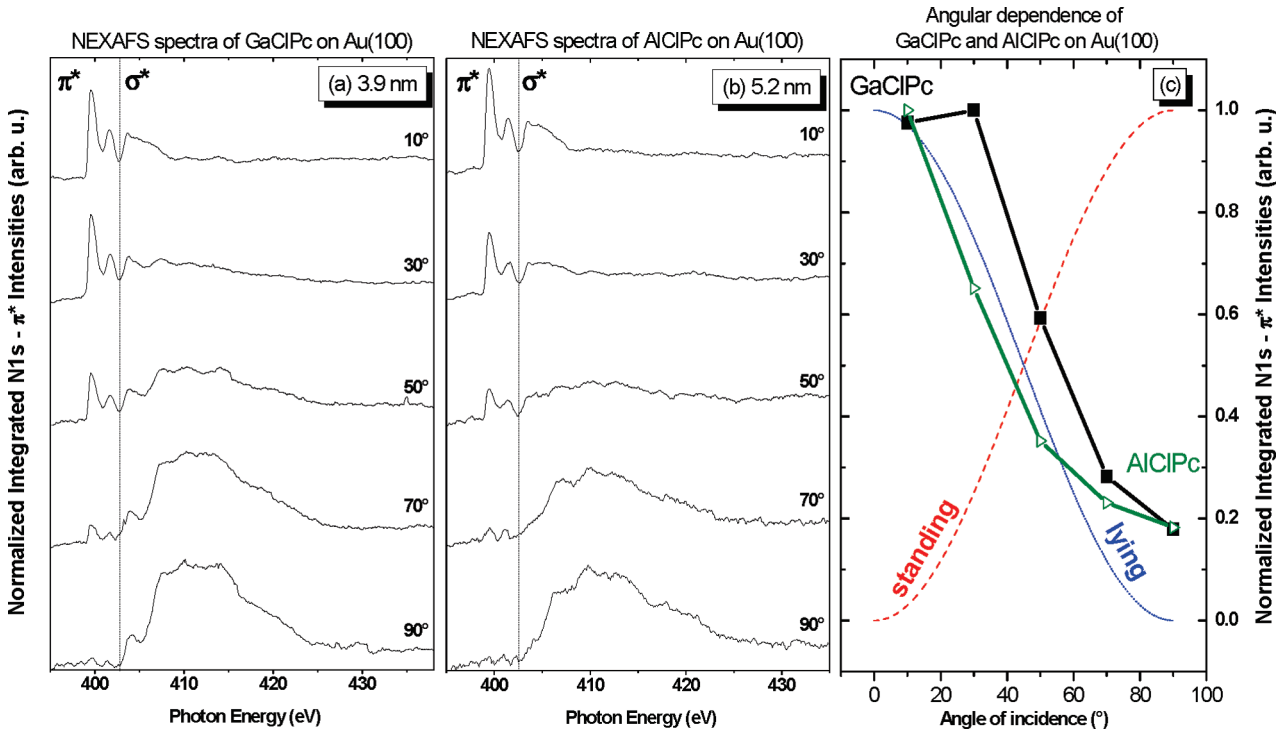

Figure 2. NEXAFS spectra of (a) GaClPc and (b) AlClPc on Au(100). The angle given in (a) and (b) denotes the incidence angle of the incoming beam. Part (c) presents the behavior of the normalized intensity with respect to the angle of incidence for GaClPc (black line) and AlClPc (green line). The red and blue lines indicate the expected functional behaviors for perfectly standing and lying molecules.

In a planar π conjugated carbon system, as in the case of planar phthalocyanines, the excitation from C 1s to a π^* orbital is allowed for **E** vertical to the molecular plane (parallel to $2p_z$), whereas the transition to σ^* is allowed for **E** parallel to the molecular plane and to the chemical bond. This also holds for N 1s if the nitrogen is in the plane of the carbon system. Thus, the molecular orientation can be probed by monitoring the relative intensities of excitations from occupied core levels into unoccupied molecular levels, either due to the rotation of the sample or, alternatively, by changing the direction of the **E** vector of the synchrotron radiation.

In the case of p-polarized light and in the lack of preferential azimuthal orientation, the dependence of the measured TEY intensities on the angle of incidence δ between surface and molecular plane can be expressed by the following equation:[42]

$$I \sim (P \cdot \sin^2 \alpha \cdot \sin^2 \delta + 2 \cdot \cos^2 \alpha \cdot \cos^2 \delta) + (1 - P) \cdot \sin^2 \alpha \quad (1)$$

In this equation, P is the polarization degree of the incoming radiation and α the angle between substrate surface and sample plane. Assuming $P = 1$ and perfectly lying and standing molecules, the expected function is reduced to a simple $\cos^2 \delta$ or $\sin^2 \delta$ function as plotted in Figures 2, 3c. These figures show the expected intensity evolution for the extreme cases of exactly lying (dotted line) and standing molecules (dashed line). Also drawn are the experimentally determined intensities for the GaClPc and AlClPc molecules on Au(100) (rectangles) and ITO (triangles). The obtained normalized intensities can be therefore compared with the expected evolution for lying and standing molecules in order to see which calculated trend fits better to the experiment. In addition, these two molecules are not perfectly flat like CuPc or ZnPc. The "umbrella-like" molecular plane is tilted by approximately 7° relative to planar phthalocyanines which is also known for other metal substituted Pcs like TiOPc.[43] In this case the expected tilt angle of the molecular π system relative to the substrate surface is for perfectly lying molecules approximately 7°. In comparison to flat Pcs, nonvanishing N 1s $\rightarrow \pi^*$ intensities are expected for lying molecules.

3.2. Raman Spectroscopy. GaClPc and AlClPc molecules possess C_{4v} symmetry. The 58 atoms per molecule lead to 168 vibrations which can be divided through normal coordinate analysis into the following molecular vibrational modes:

$$\Gamma_{irr}(\mathrm{MClPc}) = 23A_1 + 19A_2 + 21B_1 + 21B_2 + 42E \quad (2)$$

The A_2 modes are Raman inactive, and E modes show very low intensities. From A_1, B_1, and B_2 modes the orientation can be extracted. In the work presented here we apply the model of Aroca[44] to investigate the molecular orientation. Another model by Basova et al. uses Cartesian coordinates to describe the molecular orientation.[5,45−47] The appropriate angles can easily be transformed between the coordination systems by comparison of coefficients of the transformation matrices.

In the Arocas model Euler angles (ψ, θ, φ) are used to describe the molecular orientation, which was also applied by other groups to study, for example, DiMePTCDI[48,49] or sapphire single crystals.[50] Figure 1c shows the Euler angles and the rotation axis of this model. The angle φ describes a rotation around an arbitrary global Z-axis (e.g., a substrate normal), angle θ describes a tilt angle between the molecular Z' and a global Z-axis (rotation around X'), and ψ describes a rotation around the molecular Z'-axis. In this work, the global Z-axis is equal to the substrate normal as in the case of the NEXAFS experiment. In this context, the Euler tilt angle θ from the Raman experiment is

dx.doi.org/10.1021/jp202412y |J. Phys. Chem. C XXXX, XXX, 000–000

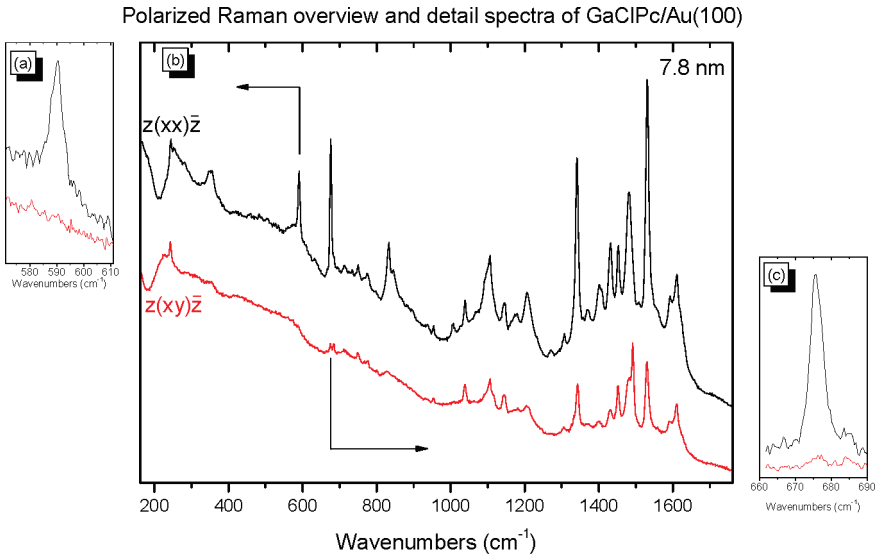

Figure 3. Polarized Raman spectra of GaClPc/Au(100) (7.8 nm): (a) detail spectra of the band at 590 cm^{-1} with $\rho \approx 0$, (b) overview spectra, and (c) detail spectra of the band at 676 cm^{-1} with $\rho = 0.02$.

equal to the angle α between the substrate surface and the sample plane in the NEXAFS experiment.

The intensity of scattered light in Raman spectroscopy is proportional to the squared change of polarizability relative to the change of normal coordinates:

$$I \sim \left(\frac{\partial \alpha}{\partial q_i}\right)^2 \tag{3}$$

α indicates the tensor element of the polarizability matrix. According to Loudon,[51] the polarizability matrix can be subdivided into its single symmetry races. The A_1 symmetry is sensitive for the tilt angle relative to the substrate surface, and we focus on the A_1 bands at 591 and 676 cm^{-1}. The polarizability tensor for A_1 modes as listed beneath is

$$\mathbf{A}_1 = \begin{pmatrix} a & 0 & 0 \\ 0 & a & 0 \\ 0 & 0 & b \end{pmatrix} \tag{4}$$

The tensor shall represent the orientation of the molecule. First, a transformation from molecular to substrate coordinates is necessary using the Euler transformation matrices in *x*-convention

$$\mathbf{R}(\varphi) = \begin{pmatrix} \cos(\varphi) & \sin(\varphi) & 0 \\ -\sin(\varphi) & \cos(\varphi) & 0 \\ 0 & 0 & 1 \end{pmatrix};$$

$$\mathbf{R}(\theta) = \begin{pmatrix} 1 & 0 & 0 \\ 0 & \cos(\theta) & \sin(\theta) \\ 0 & -\sin(\theta) & \cos(\theta) \end{pmatrix};$$

$$\mathbf{R}(\psi) = \begin{pmatrix} \cos(\psi) & \sin(\psi) & 0 \\ -\sin(\psi) & \cos(\psi) & 0 \\ 0 & 0 & 1 \end{pmatrix} \tag{5}$$

and

$$\mathbf{R} = \mathbf{R}(\varphi)\mathbf{R}(\theta)\mathbf{R}(\psi) \tag{6}$$

The transformation to substrate coordinates follows consequently

$$\mathbf{A}_1^{\text{sub}} = \mathbf{R}(\varphi, \theta, \psi)^{\mathrm{T}} \cdot \mathbf{A}_1 \cdot \mathbf{R}(\varphi, \theta, \psi) \tag{7}$$

In order to describe our experiment, randomly oriented molecules around the global *z*-axis (φ angle) are assumed. Therefore, integrations over φ for a full 2π rotation for both polarization directions are necessary.

$$I_{||/\perp} = \int_0^{2\pi} (e_i^{||} \cdot A_1^{||/\perp}(\varphi, \theta, \psi) \cdot e_s^{||/\perp})^2 \, \mathrm{d}\varphi \tag{8}$$

Using e_i and e_s, the electric unit vectors of the incident (i) and scattered (s) light with respect to the polarization (*xx* and *xy*), we can extract the proper component attributed to the geometry (in Porto notation[52] $z(xx)\bar{z}$; (||) and $z(xy)\bar{z}$; (⊥)). The angular averaging is compatible to the performed analysis of NEXAFS data above, because eq 1 also adopts the assumption of azimuthally averaged molecular orientations. Otherwise, for azimuthally well-defined molecular orientations such dependencies using Raman spectroscopy need to be included, too.[44,49,50] The coordinate system is chosen in a way that the *z*-axis of the laboratory system coincides with the substrate normal. For Au(100) this axis is parallel to the [100] direction. The obtained intensities are then inserted into the definition of the depolarization ratio:

$$\rho = \frac{I_\perp}{I_{||}} \tag{9}$$

The derived full expressions are too long to be displayed in detail. However, the angular dependence of the depolarization ratio can be simplified to

$$\rho \propto \sin^4 \theta \tag{10}$$

for A_1 modes. Additionally, the tensor element *a* is expected to be much larger than *b*, due to the fact that the polarizability in the phthalocyanine ring (approximately the *xy*-plane) is much larger

dx.doi.org/10.1021/jp202412y |*J. Phys. Chem. C* XXXX, XXX, 000–000

than in the z-direction (Ga−Cl bonding). Thus, in a first approximation one can set $a = 1$ and $b = 0$. In this case lying molecules are expected with a depolarization ratio of 0 and standing molecules with a ratio of 1/3, respectively.

To evaluate the depolarization ratio, the background has to be subtracted and the integral peak intensity is determined by numerical integration of the peak area. Further, the depolarization of the scattered light, which arises from film inhomogeneity, is neglected.

4. RESULTS AND DISCUSSION

Au(100) may exhibit multiple reconstructions, whereas the (5×20) pattern is the most prominent, respectively. This surface reconstruction is also present in our experiments, although more complex reconstructions are possible.[53] In comparison, the surface of ITO is quite rough. The ITO surface is also sensitive to the preparation method.[54] Sputtering is known to preferentially decrease surface oxygen and thus reduce the oxidation state of the metal atoms, and it is also known to induce roughening. Treatments with HCl or ozone may also significantly change the surface structure. Here, we cleaned ITO by thermal annealing in UHV.

First, we will present and discuss the experimental data of both molecules on Au(100). In Figure 2a, b the X-ray excitation spectra from N 1s into unoccupied states are depicted for five incidence angles δ of the p-polarized synchrotron radiation between 10 and 90°. In this case $\delta = 10°$ corresponds to nearly grazing incidence and $\delta = 90°$ to normal incidence. Spectral features at photon energies <402 eV correspond to N 1s → π^* transitions and at >402 eV to N 1s → σ^* transitions.[16,38] There are clearly visible angular dependencies of the π^* resonances with a maximum intensity at grazing incidence ($\delta = 10°$) and a maximum for the σ^* resonances at normal incidence ($\delta = 90°$). This fits well to lying molecules.[16] The transition into π^* states is expected to possess a minimum if the electric field vector **E** is perpendicular to the surface normal (i.e., in the plane of the π-conjugated system). A small overlap of the incoming electrical field vector **E** with the dipolar transition moment results in small (or vanishing) intensities for resonances into π^* states. This behavior is apparent if the electric vector **E** lies perpendicular to the surface normal. Transitions into σ^* states can be observed with contrary angular evolution. Figure 2c shows the complete evolution of the normalized integrated π^* intensity drawn as a function of the inclination angle δ. For both, GaClPc (3.9 nm) and AlClPc (5.2 nm) films, the data for the Au(100) substrate fit well with the expected trend for lying molecules. The observed angular dependencies of the N 1s → π^*, σ^* transitions of GaClPc and AlClPc on Au(100) therefore indicate preferred lying molecules. For these two systems (GaClPc and AlClPc on Au(100)), the molecular "plane" aligns parallel to the surface. This behavior is also observed for flat Pcs like CuPc on polycrystalline and single crystalline Au as well as for peripherally substituted planar Pcs on the same substrates.[16] The difference from the metal substituted phthalocyanines investigated here is the existence of a permanent dipole moment.

In order to obtain independent information on the molecular orientation, we performed in addition experiments using Raman spectroscopy. Here, we focus on GaClPc on the two different substrates. Figure 3 represents the overview and detail spectra of GaClPc/Au(100) with a nominal film thickness of 7.8 nm. We chose the A_1 bands at 590 and 676 cm^{-1} for orientation analysis since these two modes are well separated from other bands and the uncertainty due to background correction and band overlap is much smaller than in other regions, e.g., >1000 cm^{-1}. However, the A_1 band at 676 cm^{-1} possesses a very weak shoulder which can be related to another symmetry (E). In principle, it is also possible to calculate the orientation from bands of different symmetry (e.g., B_1 and B_2). Since the A_1 symmetry modes exhibit a distinct dependence of the depolarization ratio on the orientation, they are well suited for the analysis of the molecular tilt angle with respect to substrate normal in thin films.

The overview spectra are recorded in both parallel $z(xx)\bar{z}$; and perpendicular $z(xy)\bar{z}$; polarization and are drawn in Figure 3b. The background consists of fluorescence excited from the gold. The absence of pronounced gold bands facilitates the band evaluation. The two interesting bands are drawn in Figure 3a, c. The depolarization ratios are determined to be close to 0.00 for the band at 590 cm^{-1} and 0.02 ± 0.01 at 676 cm^{-1}, respectively. The Euler angles θ related to these depolarization ratios (including uncertainties) are in the range between 0° and 30° ($\rho = 0$ for lying and 1/3 for standing molecules for systems) and suggest essentially lying molecules. This rather large uncertainty results from the $\sin^4(\theta)$ dependency which hardly gives differences in ρ within this angular range because of the slight slope.

Results of Raman spectroscopy measurements agree well with NEXAFS and predict a similar, essentially lying molecular orientation based on the discussion above. The same holds for AlClPc on Au(100). We note that the molecular orientation can be a function of the film thickness. This is in particular observed on non-single-crystalline surfaces, where the orientation changes after the growth of 2−4 monolayers from "lying" to "standing".[16,56] For phthalocyanines on single crystalline gold, on the other hand, it is well-known that the molecules can maintain their (lying) orientation from the interface into the bulk for several tenths of nanometers.[16,55] The different growth modes observed on various substrates can be understood in terms of different molecule−substrate and molecule−molecule interactions, discussed in detail in ref 56. Since the film thickness for XAS and Raman measurements is similar, we suppose that it is not necessary to consider thickness dependent variations of the orientation in the discussion above.

On ITO substrates the situation appears quite different compared to the Au(100) substrate. The angle dependent N 1s → π^* NEXAFS spectra for the GaClPc (3.8 nm) and AlClPc (6.3 nm) films are shown in Figure 4a, b, and the normalized integrated intensities with respect to the incidence of the electric field vector **E** are presented in Figure 4c. For both molecules the π^* intensities do not show a clear angular dependence. This may be explained by differently oriented domains, by different molecular orientations (disordered films), or by an average tilt angle close to the magic angle (54.7°). From the NEXAFS spectra, it is therefore unclear if the mean angle is related to different oriented molecules or layers. Raman measurements (Figure 5) and depolarization ratios related to GaClPc on ITO predict a similar result. In the overview, spectra signals arising from the ITO are clearly visible. The strong background in the range of 200−650 and 850−1250 cm^{-1} is related to the ITO substrate. The same GaClPc bands are used for orientation analysis as in the case of films on Au(100). The depolarization ratios of the A_1 bands can be determined to be 0.14 ± 0.06 and 0.17 ± 0.05 for the bands at 590 and 676 cm^{-1}. Tilt angles of 50−70° can be assigned to these values, and they also fall in a range close to the magic angle. The $\sin^4(\theta)$ function possesses a

dx.doi.org/10.1021/jp202412y |J. Phys. Chem. C XXXX, XXX, 000–000

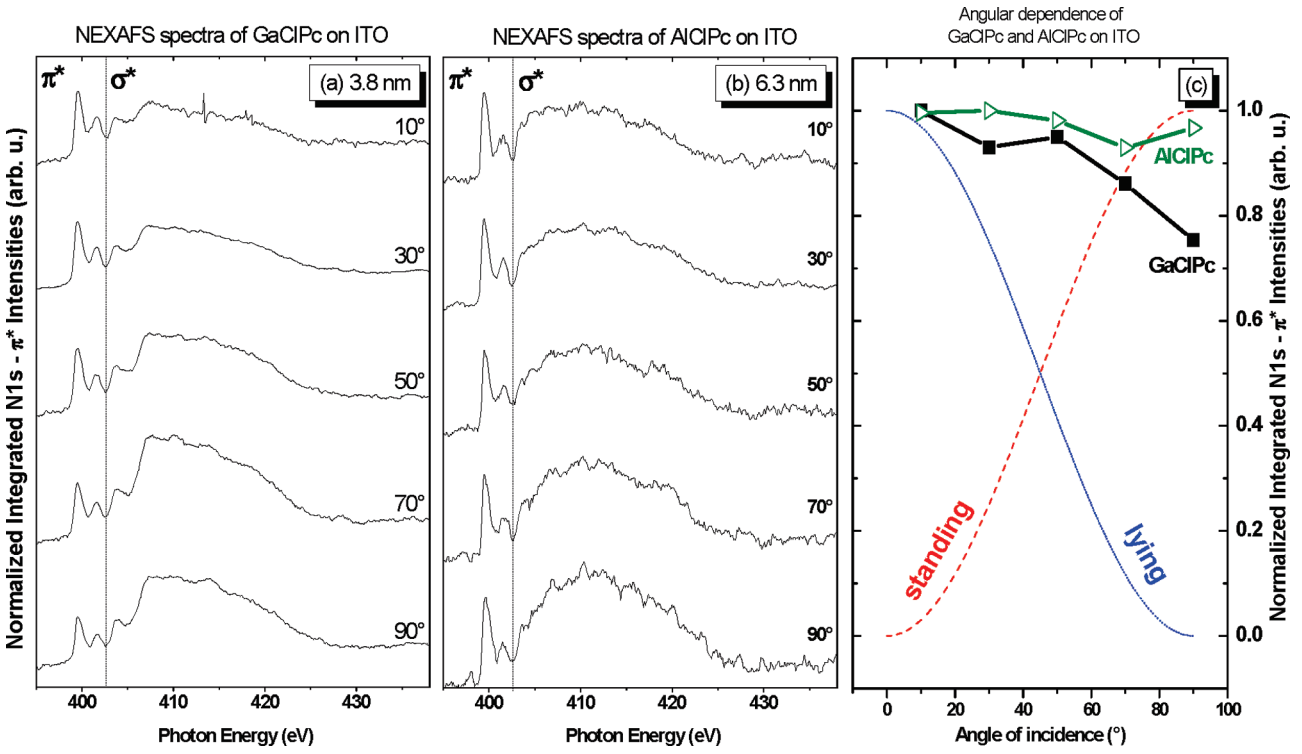

Figure 4. NEXAFS spectra of (a) GaClPc and (b) AlClPc on ITO. The angle given in (a) and (b) denotes the incidence angle of the incoming beam. Part (c) presents the behavior of the normalized intensity with respect to the angle of incidence for GaClPc (black line) and AlClPc (green line). The red and blue lines indicate the expected function for perfectly lying and standing molecules.

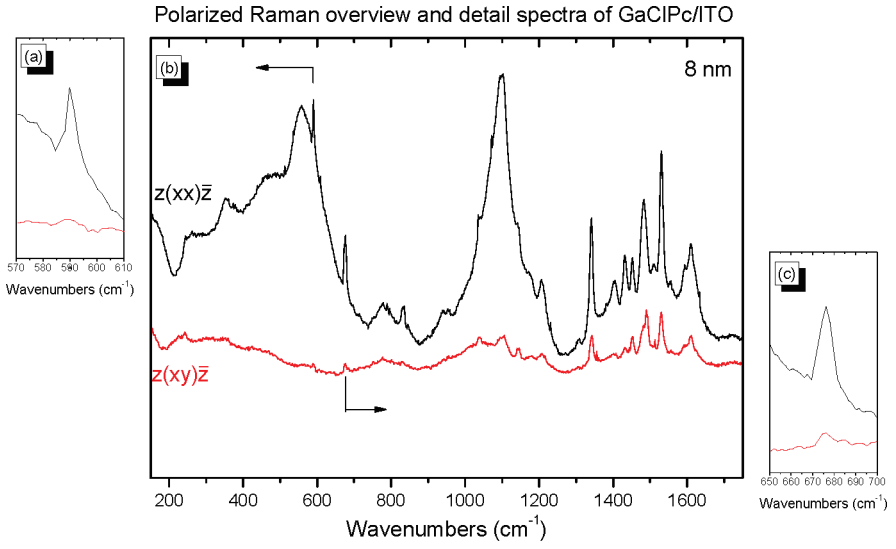

Figure 5. Polarized Raman spectra of GaClPc/ITO (8 nm). (a) Detail spectra of the band at 590 cm^{-1} with $\rho = 0.17$, (b) overview spectra, and (c) detail spectra of the band at 676 cm^{-1} with $\rho = 0.18$.

much larger slope in the molecular tilt angle range between 45° and 70°, which results in a larger sensitivity. These data represent an average of several spectra since these ratios can vary to some extent due to the condition of the substrate morphology (e.g., if the molecule or layer is attached to a valley or a hill). A representative set of spectra is shown in Figure 5. The assigned depolarization ratios in Figure 5 are related to these spectra. However, these data compared to those from ref 26 are different since the electrical field influences the molecular orientation. In this manner, the Raman data seem to support the proposal of tilted molecular arrangement in the films on ITO derived from the NEXAFS data to some extent, but more information seems necessary.

In order to study this problem in more detail, Raman intensity mapping using the confocal microscope is performed. Raman intensity maps on 25 × 25 μm^2 areas have been recorded from GaClPc films on Au(100) and ITO, and they have been displayed in parts a and b, respectively, of Figure 6. The figures depict the

dx.doi.org/10.1021/jp202412y |J. Phys. Chem. C XXXX, XXX, 000–000

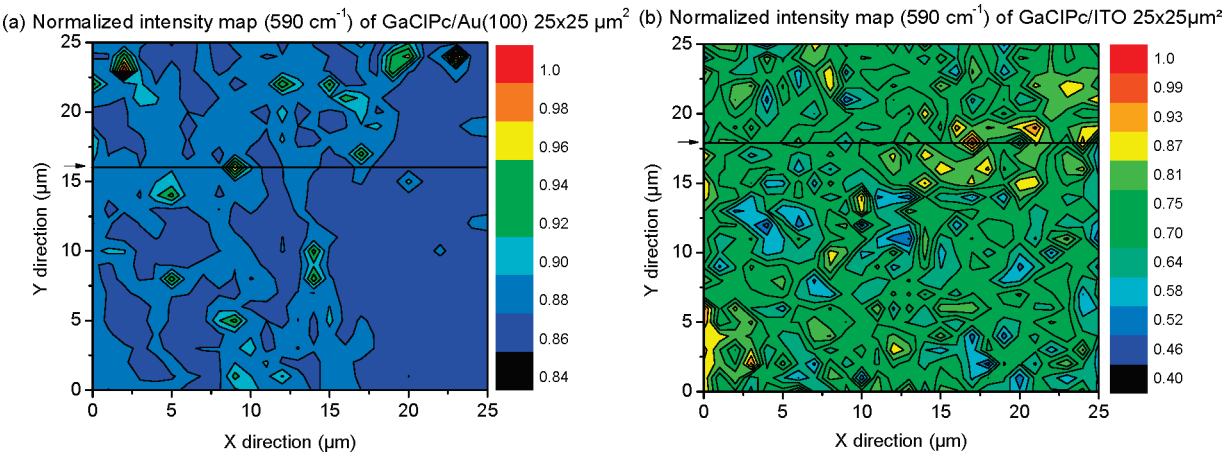

Figure 6. (a) Image of a 25 × 25 μm^2 mapped area of GaClPc/Au(100) and (b) on ITO. In both cases the A_1 mode at 590 cm^{-1} is used to probe the film homogeneity. The normalized intensity variation is displayed as a function of the position.

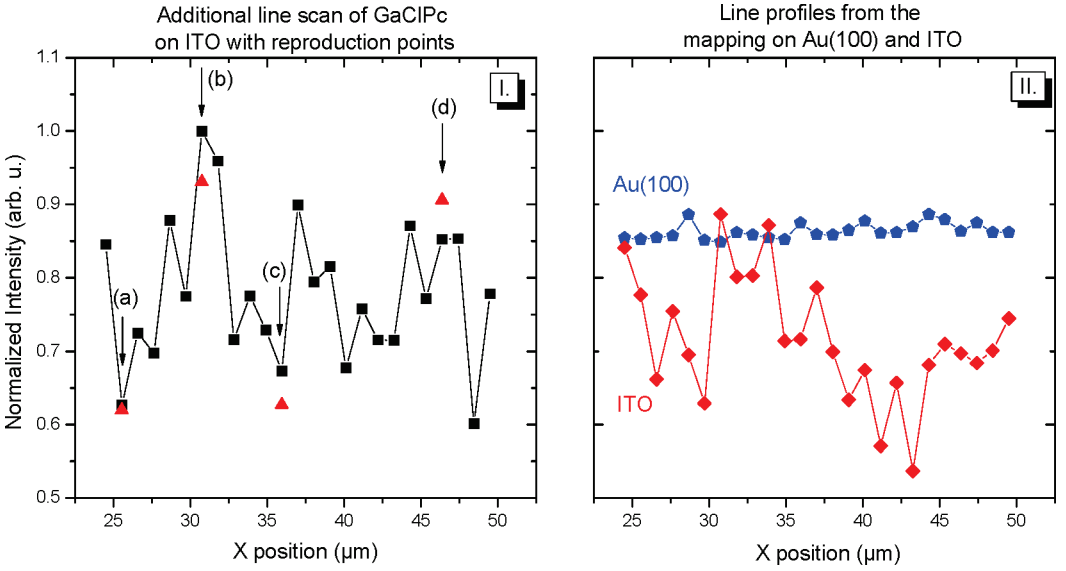

Figure 7. (I) Raman line scan in the *x*-direction of GaClPc/ITO. The intensity profile corresponds to the normalized peak area of the A_1 mode at 590 cm^{-1}. The depolarization ratio and therefore the tilt angle *q* are determined at the points a−d. The triangular points correspond to points for testing the reproduction of the position. The orientations at the specific points are (a) 78°, (b) 64°, (c) 68°, and (d) 90°. (II) Line profiles of the mapping of GaClPc on Au(100) (blue) and ITO (red) taken from Figure 6a, b. The taken profiles are marked in the color plots by black lines.

normalized integral intensities of the A_1 mode at 590 cm^{-1} as function of the positions (*x*, *y*) on the surfaces. From these measurements, information related to morphology of the thin film can be extracted. Looking at the whole image in Figure 6a, only a weak variation of the intensities is observed indicating a laterally rather homogeneous film. Some localized spots possess higher intensities and can be interpreted as single islands, tentatively. Changes in the intensities are small on the order of a few percent. Judging from the color scale, much larger intensity variations may be observed in Figure 6b, which represents the Raman image recorded on ITO. This seems to point to laterally much more inhomogeneous films on ITO. However, the locally measured intensities are affected by both layer thickness and molecular orientations. Thus, also the depolarization ratios have been determined for all local spots within the images. In brief, at all the measured spots the depolarization ratios and hence the related tilt angles vary only in narrow ranges typical for either part a or b of Figure 6. This holds for arbitrary positions in films but also for the spots with highest intensity (islands). There is no evidence for differently oriented domains in these data, and the conclusion that the observed Raman data likely correspond to particular molecular orientations in the films can be made. But of course, the discrimination of domains smaller than the lateral resolution of our Raman system here cannot be done. On the other hand, islands with apparent widths of 2−4 μm can be clearly recognized in both of the images. In the case of the investigated films, the lateral intensity variations evidently reflect the variations in film thickness quite well. The thickness information is independent of the roughness of the substrate below, quite contrary to thickness information derived from AFM. In case of AFM studies, the substrate roughness may severely affect the information on film thickness and film roughness.

Further detailed comparison of the films on the different substrates may be performed by comparing line scans taken

dx.doi.org/10.1021/jp202412y |*J. Phys. Chem. C* XXXX, XXX, 000–000

separately from other areas of the film (Figure 7a, GaClPc on ITO) or line scans taken from the lateral images (Figure 7b, GaClPc on Au(100) and on ITO). The Raman intensity in Figure 7a has been normalized to the maximum intensity measured along this individual line, while the intensities in Figure 7b have been normalized to the highest intensity measured in the related Raman image (6a or b). The line scans from films on ITO exhibit similar strong intensity variations, demonstrating the rather inhomogeneous GaClPc thickness on this rough substrate. The detected intensity changes partly by a factor of 2. Many isolated islands and edges can be discriminated from neighboring structures within the resolution conditions. For fast and qualitative discussions, Raman imaging provides a useful tool to support statements about surfaces and qualitative discussions about the growth mode.

On the contrary, the quite smooth Raman intensity profile obtained from GaClPc on Au(100) fits again to a very homogeneous film on this surface.

In this manner, information obtained from Raman imaging points also to a quite different morphology of the films on the two substrates. In the case of the investigated films on the Au(100) single crystal surface, essentially flat lying molecules and a smooth film surface have been found. On the other hand, in spectroscopic results obtained from the film on the rough ITO substrate, average tilt angles clearly point to an upright tilted molecular orientation or to a disordered growth which cannot be laterally resolved, and to a rather rough film surface. These results for nonplanar Pc molecules may be compared to those obtained for planar Pc molecules on atomically flat single crystalline metal (Au(100)) substrates or on either rough, polycrystalline metal substrates (Au) or rough ITO.[19,55] The interaction of the molecular dipole moments of these nonplanar molecules with substrate surface or other molecular dipoles evidently does not significantly affect the general tendency in molecular film growth in relation to surface roughness. Furthermore, the difference in molecular orientation between lying and tilted or standing molecules is expected to affect the diffusion processes accompanying the growth of the films. This will have implications for the formation of flat layers or islands and thus on flat or islandlike film growth modes, which are clearly reflected in the results presented above.

5. CONCLUSIONS

Thin films of nonplanar phthalocyanines GaClPc and AlClPc, which possess significant molecular dipole moments, have been prepared on a model substrate (Au(100)) and on technically relevant ITO). NEXAFS and Raman spectroscopy were combined to probe the orientation of the thin films. Both methods yield quite similar results. On Au(100), lying molecules have been observed with NEXAFS and Raman spectroscopy, and the presence of a significantly flat film surface has been concluded from Raman imaging. On the other hand, on wet chemically cleaned ITO, average tilt angles point to an upright tilted molecular orientation or to a disordered growth on this rough substrate. The results are similar to those from previous ones on planar Pc molecule films on flat or rough substrates despite the difference in dipole moments and molecular structure.

Further, we have successfully demonstrated the possibility to probe the orientation of molecular Pc films with thicknesses below 10 nm with Raman spectroscopy.

Raman imaging permits access to local information on both the molecular orientation and the film thickness—even for thicknesses below 10 nm. Since for such thin films AFM maps mainly the substrate roughness, Raman imaging becomes an interesting tool for the independent determination of the local thickness of the organic film and the morphology. A broad variation of the film thickness has been found on ITO; the local molecular orientation, however, is independent of the thickness.

AUTHOR INFORMATION

Corresponding Author

*E-mail florian.latteyer@uni-tuebingen.de; tel. (+49) 07071 2977864; fax (+49) 07071 295490.

ACKNOWLEDGMENT

We thank W. Neu and H. Löchel for technical assistance. Financial support by the University of Tübingen Corporate research group "Bacteria-Materials-Interactions" and the German Research Council Ch 132/20-1 and financial travel support by BESSY are gratefully acknowledged. We also acknowledge the electron storage ring BESSY II for provision of synchrotron radiation at the Optics-beamline.

REFERENCES

(1) Armstrong, N. R.; Wang, W. N.; Alloway, D. M.; Placencia, D.; Ratcliff, E.; Brumbach, M. *Macromol. Rapid Commun.* **2009**, *30*, 717–731.
(2) Kim, D. Y.; So, F.; Gao, Y. L. *Sol. Energy Mater. Sol. Cells* **2009**, *93*, 1688–1691.
(3) Peumans, P.; Yakimov, A.; Forrest, S. R. *J. Appl. Phys.* **2003**, *93*, 3693–3723.
(4) Jie, Z.; Li-Hua, H.; Shan, G.; Hui, Z.; Jing-Gui, Z.; Ning, L. *Sens. Actuators, A* **2007**, *126*, 588–594.
(5) Basova, T. V.; Kol'tsov, E. K.; Igumenov, I. K. *Sens. Actuators, B* **2005**, *105*, 259–265.
(6) Liu, C. J.; Wang, S. Y.; Hsieh, J. C.; Ju, Y. H. *Sens. Actuators, B* **2000**, *65*, 371–374.
(7) Horowitz, G.; Hajlaoui, M. E. *Adv. Mater.* **2000**, *12*, 1046–1050.
(8) Horowitz, G. *Adv. Mater.* **1998**, *10*, 365–377.
(9) Amsalem, P.; Giovanelli, L.; Themlin, J. M.; Angot, T. *Phys. Rev. B* **2009**, *79*, 235426.
(10) Shahrokhian, S.; Yazdani, J. *Electrochim. Acta* **2003**, *48*, 4143–4148.
(11) Petraki, F.; Peisert, H.; Biswas, I.; Chassé, T. *J. Phys. Chem. C* **2010**, *114*, 17638–17643.
(12) Peisert, H.; Kolacyak, D.; Chassé, T. *J. Phys. Chem. C* **2009**, *113*, 19244–19250.
(13) Zhang, L.; Peisert, H.; Biswas, I.; Knupfer, M.; Batchelor, D.; Chassé, T. *Surf. Sci.* **2005**, *596*, 98–107.
(14) Wang, L.; Qi, D. C.; Liu, L.; Chen, S.; Gao, X. Y.; Wee, A. T. S. *J. Phys. Chem. C* **2007**, *111*, 3454–3458.
(15) Schuster, B. E.; Basova, T. V.; Peisert, H.; Chassé, T. *ChemPhysChem* **2009**, *10*, 1874–1881.
(16) Peisert, H.; Biswas, I.; Knupfer, M.; Chassé, T. *Phys. Status Solidi B* **2009**, *246*, 1529–1545.
(17) Biswas, I.; Peisert, H.; Casu, M. B.; Schuster, B. E.; Nagel, P.; Merzz, M.; Schuppler, S.; Chassé, T. *Phys. Status Solidi A* **2009**, *206*, 2524–2528.
(18) Basova, T. V.; Kiselev, V. G.; Schuster, B. E.; Peisert, H.; Chassé, T. *J. Raman Spectrosc.* **2009**, *40*, 2080–2087.
(19) Biswas, I.; Peisert, H.; Nagel, M.; Casu, M. B.; Schuppler, S.; Nagel, P.; Pellegrin, E.; Chassé, T. *J. Chem. Phys.* **2007**, *126*, 174704.
(20) Huang, Y. L.; Wang, R.; Niu, T. C.; Kera, S.; Ueno, N.; Pflaum, J.; Wee, A. T. S.; Chen, W. *Chem. Commun.* **2010**, *46*, 9040–9042.
(21) Dick, S.; Peisert, H.; Dini, D.; Hanack, M.; Cook, M. J.; Chambrier, I.; Chassé, T. *J. Appl. Phys.* **2005**, *97*, 073715.

(22) Knupfer, M.; Peisert, H. *Phys. Status Solidi A* **2004**, *201*, 1055–1074.
(23) Kolacyak, D.; Peisert, H.; Chassé, T. *Appl. Phys. A: Mater. Sci. Process.* **2009**, *95*, 173–178.
(24) Aristov, V. Y.; Molodtsova, O. V.; Maslyuk, V. V.; Vyalikh, D. V.; Zhilin, V. M.; Ossipyan, Y. A.; Bredow, T.; Mertig, I.; Knupfer, M. *J. Chem. Phys.* **2008**, *128*, 034703.
(25) Figgis, B. N.; Kucharski, E. S.; Reynolds, P. A. *J. Am. Chem. Soc.* **1989**, *111*, 1683–1692.
(26) Biswas, I.; Peisert, H.; Schwieger, T.; Dini, D.; Hanack, M.; Knupfer, M.; Schmidt, T.; Chassé, T. *J. Chem. Phys.* **2005**, *122*, 064710.
(27) Basova, T. V.; Kiselev, V. G.; Plyashkevich, V. A.; Cheblakov, P. B.; Latteyer, F.; Peisert, H.; Chassè, T. *Chem. Phys.* **2011**, *380*, 40–47.
(28) Brumbach, M.; Placencia, D.; Armstrong, N. R. *J. Phys. Chem. C* **2008**, *112*, 3142–3151.
(29) Cao, L. C.; Chen, S. Y.; Wei, D. C.; Liu, Y. Q.; Fu, L.; Yu, G.; Liu, H. M.; Liu, X. Y.; Wu, D. X. *J. Mater. Chem.* **2010**, *20*, 2305–2309.
(30) Calvete, M. J. F.; Dini, D.; Hanack, M.; Sancho-Garcia, J. C.; Chen, W. Z.; Ji, W. *J. Mol. Modell.* **2006**, *12*, 543–550.
(31) Chen, J.; Li, S. Y.; Gong, F. B.; Yang, Z. P.; Wang, S. Q.; Xu, H. J.; Li, Y.; Ma, J. S.; Yang, G. Q. *J. Phys. Chem. C* **2009**, *113*, 11943–11951.
(32) Durmus, M.; Nyokong, T. *Tetrahedron* **2007**, *63*, 1385–1394.
(33) Zhang, X. F.; Xu, H. J. *J. Photochem. Photobiol., B* **1994**, *24*, 109–116.
(34) Rousseau, J.; Langlois, R.; Ali, H.; Vanlier, J. E. *J. Photochem. Photobiol., B* **1990**, *6*, 121–132.
(35) Mathew, S.; Menon, C. S.; Sudarsanakumar, C. *Optoelectron. Adv. Mater.* **2007**, *1*, 339–341.
(36) Owen, J. E.; Kenney, M. E. *Inorg. Chem.* **1962**, *1*, 331–333.
(37) Shao, Y.; Molnar, L. F.; Jung, Y.; Kussmann, J.; Ochsenfeld, C.; Brown, S. T.; Gilbert, A. T. B.; Slipchenko, L. V.; Levchenko, S. V.; O'Neill, D. P.; DiStasio, R. A.; Lochan, R. C.; Wang, T.; Beran, G. J. O.; Besley, N. A.; Herbert, J. M.; Lin, C. Y.; Van Voorhis, T.; Chien, S. H.; Sodt, A.; Steele, R. P.; Rassolov, V. A.; Maslen, P. E.; Korambath, P. P.; Adamson, R. D.; Austin, B.; Baker, J.; Byrd, E. F. C.; Dachsel, H.; Doerksen, R. J.; Dreuw, A.; Dunietz, B. D.; Dutoi, A. D.; Furlani, T. R.; Gwaltney, S. R.; Heyden, A.; Hirata, S.; Hsu, C. P.; Kedziora, G.; Khalliulin, R. Z.; Klunzinger, P.; Lee, A. M.; Lee, M. S.; Liang, W.; Lotan, I.; Nair, N.; Peters, B.; Proynov, E. I.; Pieniazek, P. A.; Rhee, Y. M.; Ritchie, J.; Rosta, E.; Sherrill, C. D.; Simmonett, A. C.; Subotnik, J. E.; Woodcock, H. L.; Zhang, W.; Bell, A. T.; Chakraborty, A. K.; Chipman, D. M.; Keil, F. J.; Warshel, A.; Hehre, W. J.; Schaefer, H. F.; Kong, J.; Krylov, A. I.; Gill, P. M. W.; Head-Gordon, M. *Phys. Chem. Chem. Phys.* **2006**, *8*, 3172–3191.
(38) Peisert, H.; Biswas, I.; Zhang, L.; Knupfer, M.; Hanack, M.; Dini, D.; Batchelor, D.; Chassé, T. *Surf. Sci.* **2006**, *600*, 4024–4029.
(39) El-Nahass, M. M.; Bahabri, F. S.; Al-Harbi, R. *Egypt. J. Solids* **2001**, *24*, 11–19.
(40) Everall, N. J. *Analyst* **2010**, *135*, 2512–2522.
(41) Meyer, M.; Etchegoin, P. G.; Le Ru, E. C. *Am. J. Phys.* **2010**, *78*, 300–306.
(42) Stöhr, J. *NEXAFS Spectroscopy*; Springer Series in Surface Sciences; Springer: Berlin, Germany, 1995.
(43) Hiller, W.; Strähle, J.; Kobel, W.; Hanack, M. *Z. Kristallogr.* **1982**, *159*, 173–183.
(44) Aroca, R.; Jennings, C.; Loutfy, R. O.; Hor, A. M. *J. Phys. Chem.* **1986**, *90*, 5255–5257.
(45) Basova, T. V.; Kolesov, B. A. *Thin Solid Films* **1998**, *325*, 140–144.
(46) Basova, T. V.; Kolesov, B. A.; Gurek, A. G.; Ahsen, V. *Thin Solid Films* **2001**, *385*, 246–251.
(47) Basova, T. V.; Durmus, M.; Gurek, A. G.; Ahsen, V.; Hassan, A. *J. Phys. Chem. C* **2009**, *113*, 19251–19257.
(48) Friedrich, M.; Gavrila, G.; Himcinschi, C.; Kampen, T. U.; Kobitski, A. Y.; Mendez, H.; Salvan, G.; Cerrillo, I.; Mendez, J.; Nicoara, N.; Baro, A. M.; Zahn, D. R. T. *J. Phys. Condens. Matter* **2003**, *15*, 2699–2718.
(49) Zahn, D. R. T.; Gavrila, G. N.; Salvan, G. *Chem. Rev.* **2007**, *107*, 1161–1232.
(50) Munisso, M. C.; Zhu, W. L.; Pezzotti, G. *Phys. Status Solidi B* **2009**, *246*, 1893–1900.
(51) Loudon, R. *Adv. Phys.* **2001**, *50*, 813–864.
(52) Damen, T. C.; Porto, S. P. S.; Tell, B. *Phys. Rev.* **1966**, *142*, 570.
(53) Wang, X. Q. *Phys. Rev. Lett.* **1991**, *67*, 3547–3550.
(54) Archambeau, S.; Seguy, I.; Jolinat, P.; Farenc, J.; Destruel, P.; Nguyen, T. P.; Bock, H.; Grelet, E. *Appl. Surf. Sci.* **2006**, *253*, 2078–2086.
(55) Peisert, H.; Schwieger, T.; Auerhammer, J. M.; Knupfer, M.; Golden, M. S.; Fink, J.; Bressler, P. R.; Mast, M. *J. Appl. Phys.* **2001**, *90*, 466–469.
(56) Peisert, H.; Liu, X.; Olligs, D.; Petr, A.; Dunsch, L.; Schmidt, T.; Chassé, T.; Knupfer, M. *J. Appl. Phys.* **2004**, *96*, 4009–4011.